pistil length (Fig. 2*b* and Table 1). Other QTLs for the two traits are shared on linkage groups D_C and E_L (Fig. 2*b*). In every case, the *M. cardinalis* allele increases the length of the stamen or pistil (Table 1).

Our mapping experiments show that for each of eight floral traits likely to play a role in reproductive isolation there is at least one major QTL accounting for more than 25% of the phenotypic variance (Fig. 2*b* and Table 1). This finding suggests that the evolution of reproductive isolation may involve genes of large effect and therefore that speciation may occur rapidly.

The floral syndrome associated with hummingbird pollination is found in 18 families and 39 genera in the flora of western North America, and in many cases has evolved from bee-pollinated ancestors[13]. One plausible scenario for the initial steps in the evolution of hummingbird pollination in *Mimulus* would include a sequence of three major mutations affecting pollinator attraction, reward and efficiency. A mutation at the *yup* locus causes carotenoid pigment deposition throughout the flower, reducing attactiveness to bumblebees by eliminating contrast between the petals and nectar guides. A second mutation at the major 'reward' QTL leads to greatly increased nectar volume and visitation by hummingbirds. A third mutation at the major QTL for pistil length improves the efficiency of pollen deposition by hummingbirds. This hypothesis for the evolution of hummingbird pollination is testable in part by introgressing the *M. cardinalis* allele at each major QTL into a *M. lewisii* genetic background (singly and in combination), followed by assessment of pollinator visitation and its fitness consequences in nature. □

Received 16 March; accepted 28 June 1995.

1. Mayr, E. *Animal Species and Evolution* (Harvard Univ. Press, Cambridge, Massachusetts, 1963).
2. Maynard Smith, J. *A. Rev. Genet.* **17,** 11–25 (1983).
3. Macnair, M. R. & Christie, P. *Heredity* **50,** 295–302 (1983).
4. Barton, N. H. & Charlesworth, B. *A. Rev. Ecol. Syst.* **15,** 133–164 (1984).
5. Gottlieb, L. D. *Am. Nat.* **123,** 681–709 (1984).
6. Coyne, J. A. *Nature* **355,** 511–515 (1992).
7. Coyne, J. A. *Evolution* **47,** 778–788 (1993).
8. Paterson, A. H. *et al. Nature* **335,** 721–726 (1988).
9. Stuber, C. W., Lincoln, S. E., Wolff, D. W., Helentjaris, T. & Lander, E. S. *Genetics* **132,** 823–839 (1992).
10. Andersson, L. *et al. Science* **263,** 1771–1774 (1994).
11. Georges, M. *et al. Genetics* **139,** 907–920 (1995).
12. Vickery, R. K. Jr in *Evolutionary Biology* (eds Hecht, M. K., Steere, W. C. & Wallace, B.) 405–507 (Plenum, New York, 1978).
13. Grant, V. *Proc. natn. Acad. Sci. U.S.A.* **91,** 10407–10411 (1994).
14. Hiesey, W. M., Nobs, M. A. & Bjorkman, O. *Carnegie Inst. Washington Publ. 628* **1,** 1–213 (Washington DC, 1971).
15. Vickery, R. K. Jr *Great Basin Naturalist* **52,** 145–148 (1992).
16. Faegri, K. & van der Pijl, L. *The Principles of Pollination Ecology* (Pergamon, New York, 1979).
17. Daumer, K. *Z. vergl. Physiol.* **41,** 49–110 (1958).
18. Kevan, P. G. in *Handbook of Experimental Pollination Biology* (eds Jones, C. E. & Little, R. J.) 3–30 (Reinhold, New York, 1983).
19. Ott, J. *Analysis of Human Genetic Linkage* (Johns Hopkins Univ. Press, Baltimore, Maryland, 1985).
20. Zeng, Z.-B. *Genetics* **136,** 1457–1468 (1994).
21. Williams, J. G. K., Kubelik, A. R., Livak, K. J., Rafalski, J. A. & Tingey, S. V. *Nucleic Acids Res.* **18,** 6531–6535 (1990).
22. Werth, C. R. *Virginia J. Sci.* **36,** 53–76 (1985).
23. Lander, E. S. *et al. Genomics* **1,** 174–181 (1987).
24. Lander, E. S. & Botstein, D. *Genetics* **121,** 185–199 (1989).
25. Hulbert, S. H. *et al. Genetics* **120,** 947–958 (1988).
26. Paterson, A. H., DeVerna, J. W., Lanini, B. & Tanksley, S. D. *Genetics* **124,** 735–742 (1990).

ACKNOWLEDGEMENTS. We thank R. K. Vickery Jr for seeds and for discussion, J. Doebley for critical review of the manuscript, J. Ramsey, M. Looyenga, M. Booth, Y. Sam and D. Ewing for technical assistance, and M. Gordon and J. Kingsolver for sharing laboratory space and equipment. This work was supported in part by the Royalty Research Fund of the University of Washington.

A reaction–diffusion wave on the skin of the marine angelfish *Pomacanthus*

Shigeru Kondo* & Rihito Asai†

* Kyoto University Centre for Molecular Biology and Genetics, Shogoin-Kawaharacho 53, Sakyo-ku, Kyoto, Japan
† Kyoto University Seto Marine Biological Laboratory, Shirahama-cho, Nishimuro-gun, Wakayama, Japan

In 1952, Turing proposed a hypothetical molecular mechanism, called the reaction–diffusion system[1], which can develop periodic patterns from an initially homogeneous state. Many theoretical models based on reaction–diffusion have been proposed to account for patterning phenomena in morphogenesis[2–4], but, as yet, there is no conclusive experimental evidence for the existence of such a system in the field of biology[5–8]. The marine angelfish, *Pomacanthus*, has stripe patterns which are not fixed in their skin. Unlike mammal skin patterns, which simply enlarge proportionally during their body growth, the stripes of *Pomacanthus* maintain the spaces between the lines by the continuous rearrangement of the patterns. Although the pattern alteration varies depending on the conformation of the stripes, a simulation program based on a Turing system can correctly predict future patterns. The striking similarity between the actual and simulated pattern rearrangement strongly suggests that a reaction–diffusion wave is a viable mechanism for the stripe pattern of *Pomacanthus*.

When juveniles of *Pomacanthus semicirculatus* are smaller than 2 cm long, they have only three dorsoventral stripes (Fig. 1*a*). As they grow, the intervals of the stripes get wider proportionally until the body length reaches 4 cm. At that stage, new stripes emerge between the original stripes (Fig. 1*b*). As a result, all the spaces between the stripes revert to that of the 2-cm juvenile. New lines are thin at first, but gradually get broader. When the body length reaches 8–9 cm, an identical process is repeated (Fig. 1*c*).

The reaction–diffusion system used here consists of two hypothetical molecules (activator and inhibitor) which control the synthesis rate of each other. Fig. 1*d* shows a computer simulation of a reaction–diffusion wave on a growing array of cells. At time 0, the field width is adjusted to be twice the intrinsic wavelength, calculated from the equations used in this simulation. One of the five cells is forced to duplicate periodically. As the field enlarges, all waves widen evenly. When the field length reaches about twice the original length, new peaks appear in the middle of the original peaks, as observed in *P. semicirculatus*, and the wavelength reverts to that of the original.

The juvenile of *P. imperator* has concentric stripes, which increase in number in a manner similar to that of *P. semicirculatus*. But when the *P. imperator* becomes an adult, the stripes become parallel to the anteroposterior axis by a process of continuous cutting and joining of the lines (data not shown). As they grow, the number of lines increases proportionally to body size, and the spaces between the lines are kept at an even width. The stripe pattern of *P. imperator* usually contains several branching points (Fig. 2*a*). During growth, the branching points move horizontally like a zip, resulting in addition of new lines. Figure 2*b–d* shows a branching point moving in the anterior direction until it fuses with the border of the stripe region. In Fig. 2*h–l*, two branching points meet and disappear leaving a new line. This type of rearrangement also happens in the simulation of the reaction–diffusion system, by setting a homologous conformation as a starting pattern (Fig. 2*e–g*, *m–q*). In Fig. 2*e*, the field height is adjusted to be six times the intrinsic wavelength. The waves in the right half are slightly extended, which

causes loss of stability in this region. The rightward movement of the branch restores the stability of the righthand region. It is notable that not only the final conformation, but also each intermediate stage (Fig. 2*n–p*), look quite similar to the actual pattern change that occurs in the fish (Fig. 2*i–k*).

Branching points located on more dorsal or ventral regions behave differently. As shown in Fig. 3*a–c*, they move vertically by switching at a joint. This phenomenon can be simulated by the program used in Figs 1 and 2 only by setting a different starting pattern (Fig. 3*d–f*). In the simulation, a local region that contains a branching point is less stable than a region without a branch point, and joint switching tends to occur. The direction of joint switching is determined by the conformation of neighbouring lines. In our simulation, the line under the branching point is straighter than the line above. Because the curving line is less stable than the straight line, the joint switches in the upper direction. If both upper and lower lines are symmetrical to the branched line, horizontal movement of the branch point occurs (Fig. 2). In the case of actual young fish, the lines in the middle region are usually straight, but in the dorsal and ventral regions the lines are curved. Branching points always move farther away from the middle region which consists of straight lines.

The times required for these pattern changes also suggest a mechanistic homology between actual fish and the simulations. In the simulation of joint switching, one change of joint can take place very quickly (in less than 1,000 iterations of calculation), because the change in pattern is quite local. For the horizontal movement of the branching point (from Fig. 2*e* to *g*), more than 50,000 iterations are required because it is necessary for the upper lines and lower lines to 'slide' in order to evolve to a new pattern of stripes that are evenly spaced. In the case of real fish, the joint changes also occur quickly. In the fastest case we have observed, it took place in two days (data not shown), whereas the change from Fig. 2*b* to *d* took more than three months.

Although we do not have any information about the molecules which are involved in the pattern-forming reaction, it is possible to estimate roughly the diffusion coefficients of the molecules by comparing the simulation and the actual pattern changing of fish stripe. The stripe spacing is ~0.5 cm in *P. imperator*, and ~10 grids in the simulated patterns (Fig. 2); a grid in the simulation therefore represents 0.05 cm. The pattern change from Fig. 2*h* to *l* took 90 days (7,776,000 seconds) in reality, and 50,000 iterations in the simulation. The time step for the simulation therefore corresponds to 155.5 seconds. These values give diffusion coefficients of 1.125×10^{7} cm^2 s^{-1} and 1.608×10^{-6} cm^2 s^{-1} for the activator and the inhibitor, respectively. Both values are in the range of the diffusion coefficients of proteins in aqueous media[9]. However, the diffusive molecules may be smaller than proteins, because the diffusion rate of molecules is usually much smaller in real biological systems than in aqueous media.

In some other biological systems, the insertion of new structures during growth have been observed and simulated[3,10 14]. The novel features of the work reported here are that the inserted structure is a stripe and that the underlying mechanism is operative for a long period. The reaction–diffusion wave is a kind of standing wave. Therefore, to determine that a given pattern is consistent with a reaction–diffusion wave, it is necessary to impose some disturbance on the field and to see how the

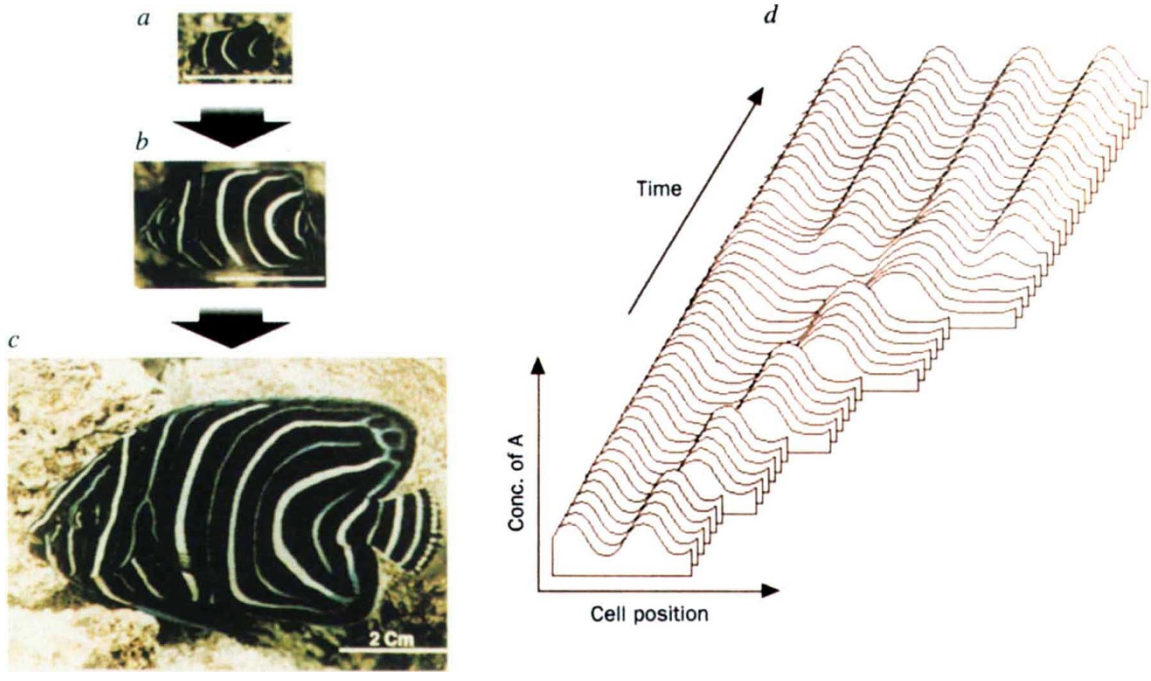

FIG. 1 Rearrangement of the stripe pattern of *Pomacanthus semicirculatus* and its computer simulation. *a–c*, Photographs of the juvenile of *P. semicirculatus*. Ages are ~2 months (*a*), ~6 months (*b*) and ~12 months (*c*). Scale bars, 2 cm. *d*, Computer simulation of the reaction–diffusion wave on the growing one-dimensional array of cells. One of the five cells is forced to duplicate periodically (once in 100 iterations). Concentration of activator is represented as the vertical height. The equations for calculation are as follows:

$$\frac{dA}{dt} = c_1 A + c_2 I + c_3 - D_A \frac{d^2 A}{dx^2} - g_A A, \quad \frac{dI}{dt} = c_4 A + c_5 - D_I \frac{d^2 I}{dx^2} - g_I I$$

where A and I are the concentration of the activator molecule and the inhibitor molecule, respectively, D_A and D_I are the diffusion constants, g_A and g_I are the decay constants, and $D_A = 0.007$, $D_I = 0.1$, $g_A = 0.03$, $g_I = 0.06$, $c_1 = 0.08$, $c_2 = -0.08$, $c_3 = 0.05$, $c_4 = 0.1$, $c_5 = -0.15$. Upper and lower limits for the synthesis rates of the activator ($c_1 A + c_2 I + c_3$) and inhibitor ($c_4 A + c_5$) are set as $0 < c_1 A + c_2 I + c_3 < 0.18$ and $0 < c_4 A + c_5 < 0.5$. These upper and lower limits are set to avoid unrealistic situations. A moderate upper-limit value of the activator synthesis rate is required to get a pattern of stripes rather than spots[15] (spots are obtained if this value is exceeded). We used the kinetics of Turing[1]. Other stripe-forming interactions[12,15], in which the upper and lower limit is a natural outcome of the kinetics, can simulate the fish pattern rearrangement reported here.

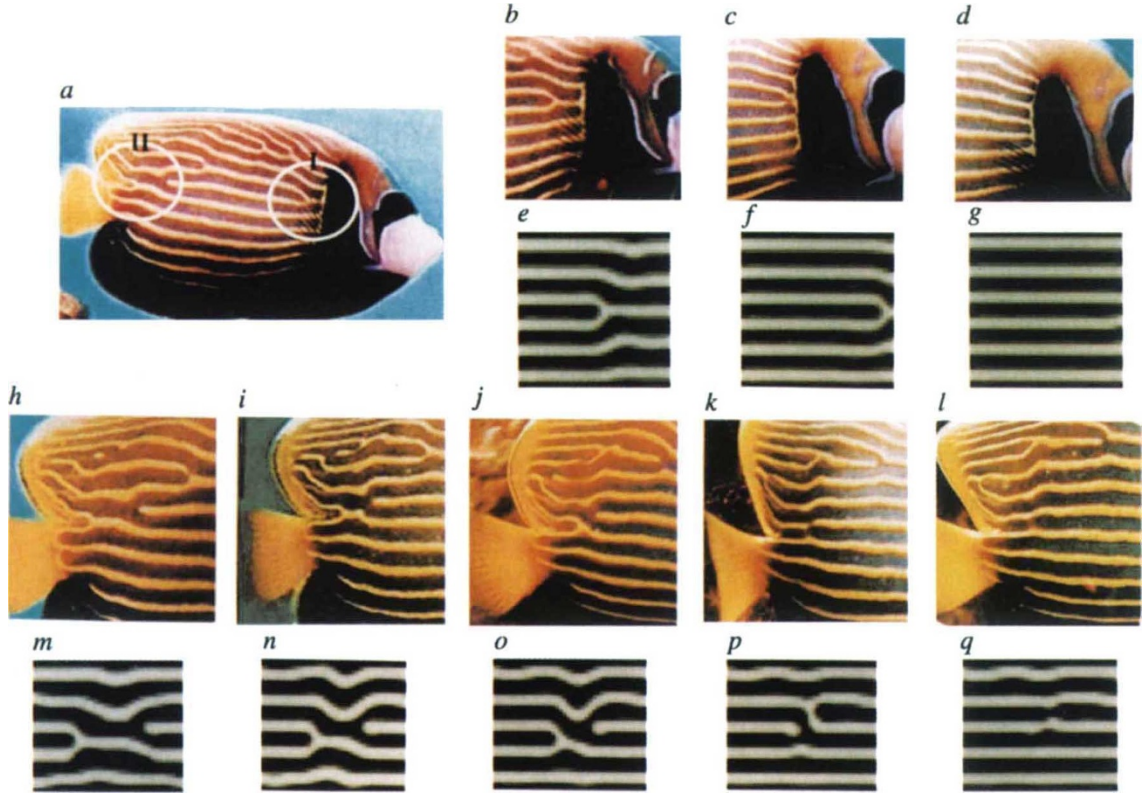

FIG. 2 Rearrangement of the stripe pattern of *Pomacanthus imperator* (horizontal movement of branching points) and its computer simulation. *a*, An adult *P. imperator* (~10 months old). *b*, Close-up of region I in *a*. *c*, *d*, Photographs of region I of the same fish taken two (*c*) and three (*d*) months later. *e*, Starting stripe conformation for the simulation (region I). *f*, *g*, Results of the calculation after 30,000 (*f*) and 50,000 (*g*) iterations. *h*, Close-up of region II in *a*. *i*–*l*, Photographs of region II of the same fish taken 30 (*i*), 50 (*j*), 75 (*k*) and 90 (*l*) days later, respectively. *m*, Starting stripe conformation for the simulation (region II). *n*–*q*, Results of the calculation after 20,000 (*n*), 30,000 (*o*), 40,000 (*p*) and 50,000 (*q*) iterations, respectively. Fish (Fish World Co. Ltd (Osaka)) were maintained in artificial sea water (Martin Art, Senju). Skin patterns were recorded with a Canon video camera and printed by a Polaroid Slide Printer. In the simulated patterns, darker colour represents higher concentrations of the activator molecule. Equations and the values of the constants used, as Fig. 1.

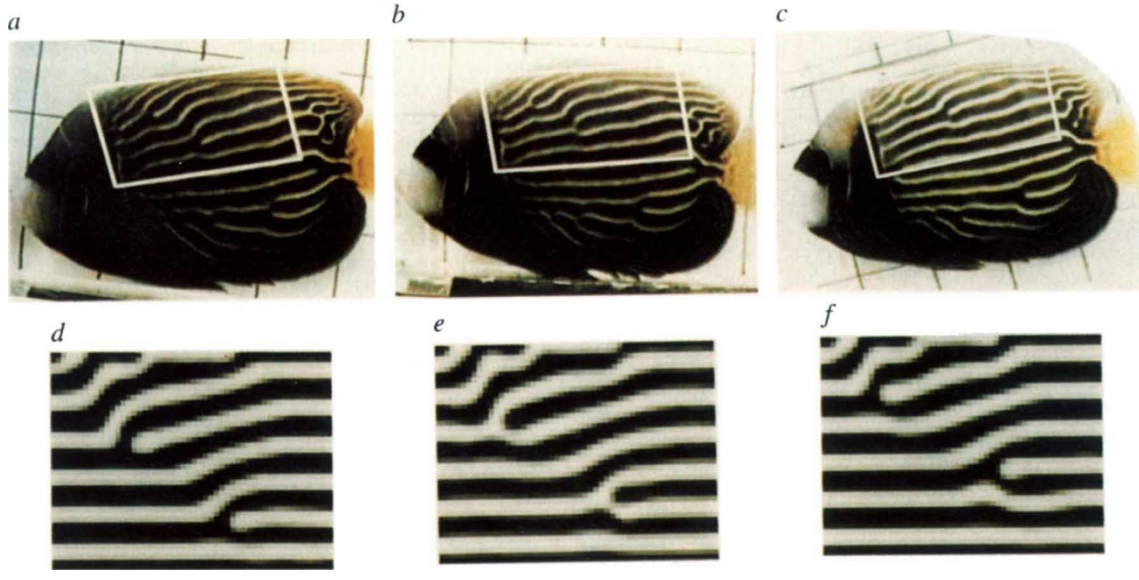

FIG. 3 Rearrangement of the stripe pattern of *P. imperator* (switch of joint) and its computer simulation. *a*, Photograph of a young *P. imperator* (~7 months old). *b*, *c*, Photographs of the same fish taken 6 (*b*) and 12 (*c*) days later. *d*, Starting stripe conformation for the simulation. Pattern changing in the region surrounded by the white box was simulated. *e*, *f*, Results of the calculation after 2,000 (*e*) and 5,000 (*f*) iterations, respectively.

pattern responds. The pattern alteration of the *Pomacanthus*, accompanied by skin growth, can be taken as a natural experiment to help elucidate the underlying mechanisms which govern pattern formation. From the striking similarity between the actual and the simulated pattern alteration, it is highly probable that the mechanism is a reaction–diffusion system. Because the pattern-forming mechanism is maintained in adult skin, it should be possible to identify the molecules involved. □

Received 19 April; accepted 15 June 1995.

1. Turing, A. M. *Phil. Trans. R. Soc.* B**237,** 37–72 (1952).
2. Kauffman, S. A. in *Pattern Formation* (eds Malacinsky, G. M. & Bryant, S.) 73–102 (Macmillan, New York, 1984).
3. Meinhardt, H. *Models of Biological Pattern Formation* (Academic, London, 1982).
4. Murray, J. D. *Scient. Am.* **258,** 80–87 (1988).
5. Winfree, A. T. *Nature* **352,** 568–569 (1991).
6. Lengyel, I. & Epstein, I. R. *Science* **251,** 650–652 (1991).
7. Ouyang, Q. & Swinney, H. L. *Nature* **352,** 610–612 (1991).
8. Pool, R. *Science* **251,** 627 (1991).
9. Dawes, E. A. *Quantitative Problems in Biology* (Longman, London, 1956).
10. Bunning, E. & Sagromsky, H. Z. *Naturf.* B**3,** 203–216 (1948).
11. Lacalli, T. C. *Phil. Trans. R. Soc.* B**294,** 547–588 (1981).
12. Meinhardt, H. *Rep. Progr. Phys.* **55,** 797–849 (1992).
13. Segel, L. A. & Jackson, J. L. *J. theor. Biol* **37,** 545–549 (1972).
14. Wigglesworth, V. B. *J. exp. Biol.* **17,** 180–200 (1940).
15. Meinhardt, H. *Development* (suppl.) **107,** 169–180 (1989).

ACKNOWLEDGEMENTS. We thank P. Maini, W. Gehring, H. Takeda and L. Ronny for discussions. We also thank A. Shimizu for the video camera and the slide printer, S. Harada for the aquarium in Seto Marine Biological Laboratory, S. Ezure for the photographs, Y. Kondo for feeding the fish, and T. Honjo for continuous encouragement and support.

Essential role for the c-*met* receptor in the migration of myogenic precursor cells into the limb bud

Friedhelm Bladt, Dieter Riethmacher, Stefan Isenmann*, Adriano Aguzzi* & Carmen Birchmeier†

Max-Delbrück-Centrum für Molekulare Medizin, Robert-Rössle-Strasse 10, 13122 Berlin, Germany
* Institut für Neuropathologie der Universität Zürich, Schmelzbergstrasse 22, 8091 Zürich, Switzerland

LIMB muscles develop from cells that migrate from the somites[1,2]. The signal that induces migration of myogenic precursor cells to the limb emanates from the mesenchyme of the limb bud[2,3]. Here we report that the c-*met*-encoded receptor tyrosine kinase is essential for migration of myogenic precursor cells into the limb anlage and for migration into diaphragm and tip of tongue. In c-*met* homozygous mutant (−/−) mouse embryos, the limb bud and diaphragm are not colonized by myogenic precursor cells and, as a consequence, skeletal muscles of the limb and diaphragm do not form. In contrast, development of the axial skeletal muscles proceeds in the absence of c-*met* signalling. The specific ligand of the c-*met* protein, the motility and growth factor scatter factor/hepatocyte growth factor[4–9], is expressed in limb mesenchyme and can thus provide the signal for migration which is received by c-*met*. We have therefore identified a paracrine signalling system that regulates migration of myogenic precursor cells.

The c-*met*-encoded receptor tyrosine kinase and its ligand, scatter factor/hepatocyte growth factor (SF/HGF), regulate growth, motility and morphogenesis of cells *in vitro*[4–10]. A targeted mutation in the SF/HGF gene causes embryonic lethality and reveals essential roles of the factor in development of liver and placenta[11,12]. To investigate cell autonomous functions of

† To whom correspondence should be addressed.

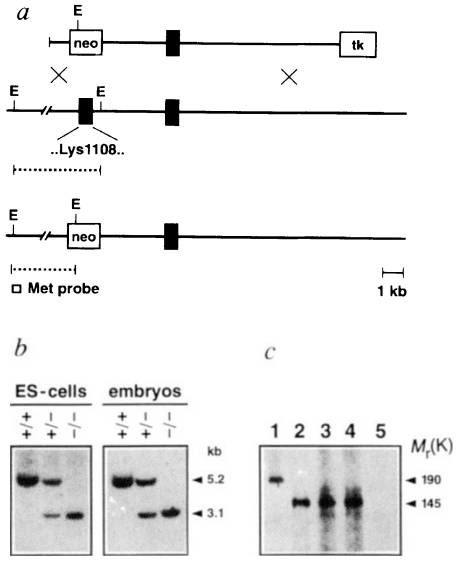

FIG. 1 Outline of the strategy to disrupt c-*met* and the effect of the mutation. *a*, Schematic representation of c-*met* targeting vector (top), wild-type c-*met* allele (middle) and mutant c-*met* allele (bottom). Exon sequences are represented by black boxes; neomycin resistance (*neo*) gene and thymidine kinase (*tk*) gene from herpes simplex[25] are shown and the triplet encoding the invariant Lys (amino acid 1,108; see ref. 26 for the numbering) is indicated. The open box indicates the probe used for Southern analysis (see *b*). Dashed lines correspond to *Eco*RI fragments detected in wild-type and mutant genomic DNA. *b*, Southern blot analysis of genomic DNA from wild-type (+/+) ES cells, from ES cells containing one (+/−) or two mutant (−/−) c-*met* alleles and from wild-type (+/+), heterozygous (+/−) and homozygous (−/−) mutant mouse embryos. *c*, *In vitro* auto-kinase assays on immunoprecipitated c-*met* protein from extracts of adult liver (c-*met* +/− animal) analysed under non-reducing (lane 1) or reducing conditions (lane 2). Auto-kinase activity of c-*met* protein immunoprecipitated from liver extracts of wild-type (+/+) (lane 3), heterozygous (+/−) (lane 4) or homozygous (−/−) embryos (lane 5) analysed under reducing conditions. In the absence or presence of reducing agents, c-*met* protein of 190 or 145K can be observed, that correspond to the α- and β-chain linked by sulphydryl bridges or to the separate β-chain, respectively. RNase protection analysis indicates that the mutant *met* allele produces normal levels of a Δ-*met* transcript that lacks nucleotides 3,254–3,334 (data not shown). METHODS. Genomic c-*met* DNA isolated from a library of 129 mouse DNA (isogenic to ES cell line E14) was used to construct two targeting vectors. One exon (nucleotides 3,254–3,334 in the cDNA) of c-*met* was replaced by either wild-type or mutant[27] *neo* gene (*neo*^{wt} or *neo*^{mu}). The targeting vector containing *neo*^{mu} was first introduced into E14-1 ES cells[28] by electroporation; homologous recombination events were enriched by selection with low G418 (0.2 mg ml^{-1}) concentrations. Two independently mutated ES cell clones (met 30; met 34) were identified. The second targeting vector containing *neo*^{wt} was electroporated into met 30 or met 34 ES cells; homologous recombination events were enriched by selection with high concentrations of G418 (1 mg ml^{-1}). Three cell clones with two mutant c-*met* alleles (met 30-1; met 34-1; met 34-2) were identified. The structure of the mutant loci and absence of additional integration events was verified by Southern hybridization. Chimaera were produced by injections of mutant ES cells into C57BL/6 blastocysts (compare also Fig. 2). Mouse strains that carry the mutation were established from met 30 and met 34 ES cells. Phenotypes were analysed on C57BL/6/129 hybrid background. For protein analysis, extracts from embryonal or adult livers were precipitated with serum against a C-terminal c-*met* peptide produced essentially as described[29]. Immunoprecipitates were incubated for 30 min, 37 °C in 15 μCi of γ-^{32}P-ATP (Amersham, 5,000 Ci mmol^{-1}), 100 mM NaCl, 20 mM HEPES, pH 7.1 (*in vitro* kinase assay) and run on a SDS–polyacrylamide gel in the presence or absence of β-mercaptoethanol.